Effect of vacancies on the structure of solid molecular parahydrogen studied with variational Monte Carlo simulations

Francesco Operetto
Dipartimento di Fisica and INFN, Università di Trento, via Sommarive, 14 I-38050 Povo, Trento, Italy

Francesco Pederiva
Dipartimento di Fisica, Università di Trento, via Sommarive, 14 I-38050 Povo, Trento, Italy
and CNR-DEMOCRITOS National Simulation Center, Trieste, Italy

(Received 5 May 2006; revised manuscript received 1 August 2006; published 2 February 2007)

We performed variational Monte Carlo simulations with a shadow wave function to study the effects of vacancies on the structure of solid molecular p-H_2. In a quantum crystal, vacancies tend to modify the local order in the crystal. The main mechanism is due to the fact that molecules tend to occupy the empty space in order to lower the kinetic energy. While this effect is expected to be more important at lower than at higher densities, we find that in the latter case the local order is even more affected by the presence of a vacancy. Results on the occurrence of quantum diffusion of the vacancy in the solid are also presented.

DOI: 10.1103/PhysRevB.75.064201 PACS number(s): 67.80.Mg

I. INTRODUCTION

Vacancies in quantum crystals originate a number of interesting effects which are absent in classical systems. Quantum diffusion of vacancies through the crystal was considered to be the mechanism that would lead to a superfluid-like behavior in solid ^{4}He.[1–3] But the presence of vacancies also influences the local order in the system, giving rise to interesting relaxation effects which are at the origin of the difference between the classical activation energy and the actual experimentally observed activation energy in ^{4}He.[4,5] Solid para-hydrogen is believed to have a behavior which is more "classical" if compared with ^{4}He, due to the much stronger attraction among molecules, which, for instance, make p-H_2 to be solid at $T=0$ K, as opposed to He, even if quantum delocalization has to be stronger due to the lighter mass. Vacancies are also indicated to play an important role in quantum diffusion of isotopic impurities embedded in a matrix of p-H_2.[6,7]

In this paper we want to address the effects of vacancies in p-H_2 crystals. Shadow wave functions[8,9] (SWF) proved to be a very efficient tool for the study of vacancies in quantum crystals. Previous results obtained for ^{4}He show, for instance, how the estimate of formation energies is in good agreement with recent results obtained by means of exact quantum Monte Carlo projective methods and with experimental data.[4,5,10]

The formation energy of a vacancy is usually schematized as the sum of three terms.[11] The leading contribution comes from the kinetic and potential energy pertaining to the particle that has been removed from the crystal. This term is essentially the vacancy formation energy in a classical rigid solid. The expression of this contribution in the thermodynamic limit is

$$\Delta E_{\mathrm{vac}}^{\mathrm{cl}} = -\frac{\langle V\rangle}{N} + Pv, \tag{1}$$

where $\langle V\rangle/N$ is the expectation value of the potential energy per particle in the system, P is the pressure and v the specific volume. The difference with the measured value can be attributed to relaxation effects in the crystal and to the diffusion of the vacancy through the crystal. The fact that in ^{4}He the SWF estimate of the formation energy is well in agreement with the experiment is an indication that such effects are included in a realistic way. An analogous estimate of the vacancy formation energy in p-H_2 has been presented in a previous work.[12]

It is commonly assumed that when pressure is increased in a quantum crystal, its behavior becomes more and more "classical." Therefore, one might expect that at high densities vacancies have a limited effect on the local order and that mobility should be almost reduced to zero. The calculations reported in this paper show instead that, at high pressure, the local distortions in the crystal due to the presence of a vacancy become dramatic.

In the next section, a brief summary of the SWF method is given. In Sec. III, results on the structural analysis and delocalization of vacancies for different values of the crystal density will be reported. Section IV is devoted to conclusions.

II. METHODS

A. Shadow wave function

The model we assume for the description of solid p-H_2 is a set of N point particles in a periodic box interacting with the Silvera-Goldman potential v_{SG}.[13] This model interaction contains an effective two-body term which approximately accounts for the triple-dipole interaction which is not negligible in p-H_2 due to the intrinsic nonspherically symmetric character of the molecule. As shown in a previous paper,[14] the truncation of the potential at the two-body level leads to a slightly inaccurate description of the equation of state, but seems not to have sizeable effects on the structural properties such as the pair distribution function. The Hamiltonian of the system is therefore

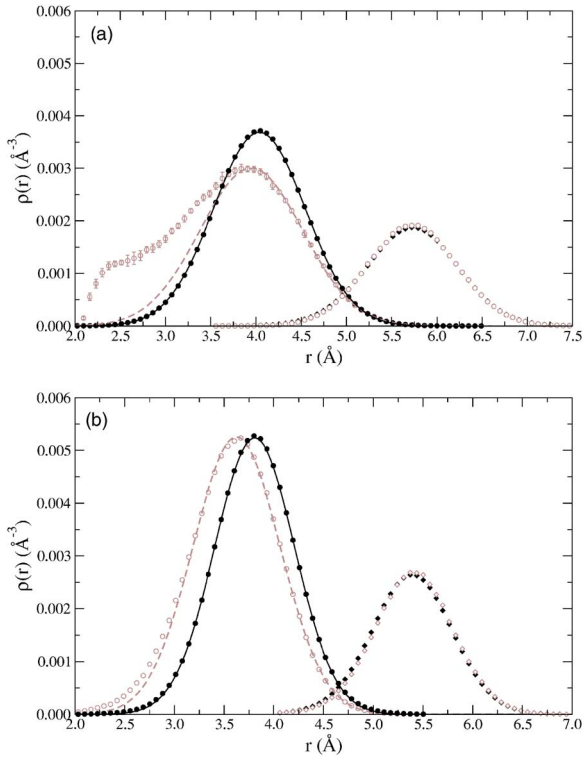

FIG. 1. (Color online) One-body density $\rho(r)$ of the first and second neighbors of a vacant (gray empty symbols) and a filled site (full black symbols) for a hcp crystal. Solid lines are Gaussian fits to first neighbors density of filled sites. Dashed curves are fitted on the right side of the density of first neighbors of the vacant sites. (a) $\rho=0.021\,50$ Å^{-3}. (b) $\rho=0.026\,00$ Å^{-3}.

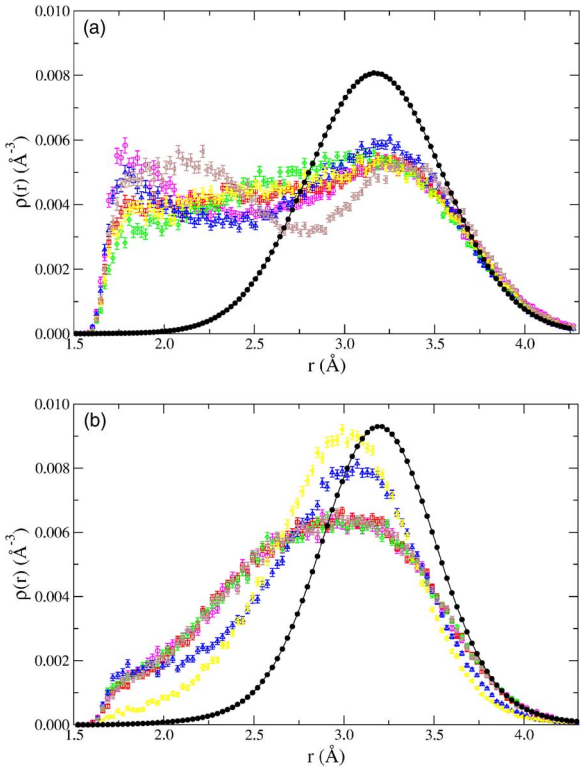

FIG. 2. (Color online) One-body density of molecules $\rho(r)$ for the first neighbors of a vacant (empty symbols) and a filled site (full symbol) at density $\rho=0.043\,00$ Å^{-3} in the fcc (a) and hcp (b) lattice. Different empty symbols refer to different MC runs. Solid lines are the average density of first neighbors of a filled site.

$$\hat{H} = -\frac{\hbar}{2m}\sum_{i=1}^{N}\nabla_i^2 + \sum_{i<j} v_{\mathrm{SG}}(r_{ij}). \tag{2}$$

The properties of the system are described by means of the variational Monte Carlo method. The estimate for the expectation of an observable of interest $\hat{O}(R)$ is obtained by sampling the square modulus of a trial solution for the time independent Schrödinger equation $\Psi_T(R)$ where $R=\{\mathbf{r}_1,\ldots,\mathbf{r}_N\}$ are the coordinates of the N molecules in the simulation cell. The approximate expectation value is given by

$$\langle O\rangle = \frac{\int dR|\Psi^*(R)|^2\hat{O}(R)}{\int dR|\Psi(R)|} \sim \frac{1}{M}\sum_{l=1}^{M} O(R_l), \tag{3}$$

where M is the number of sampled configurations.

Shadow wave functions are a particular class of trial functions which are written in integral form,

$$\Psi_T(R) = \int K(R,S)\phi_S(S)dS, \tag{4}$$

where $S=\mathbf{s}_1,\ldots,\mathbf{s}_N$ is a set of auxiliary variables, named *shadows*. The kernel $K(R,S)$, is the product of a many-body wave function of the Jastrow type, and of a product of Gaussians connecting the real and auxiliary degrees of freedom,

$$K(R,S) = \prod_{i<j}\exp\left[-\frac{1}{2}\left(\frac{b}{r_{ij}}\right)^5\right]\prod_{i=1}^{N}\exp[-C(\mathbf{r_i}-\mathbf{s_i})^2]. \tag{5}$$

The function $\phi_s(S)$ is also a many-body function of the Jastrow type, built from a pseudopotential which is just the rescaled Silvera-Goldman interaction

$$\phi_s(S) = \prod_{i<j}\exp[-\delta v_{\mathrm{SG}}(\alpha s_{ij})]. \tag{6}$$

The parameters b, C, δ, and α have been determined by minimizing a combination of the expectation value of the Hamiltonian $\hat{H}$ and of its variance $\sigma^2(\hat{H})$[12] on a set of configurations sampled from

$$\Xi(R,S,S') = K(R,S)K(R,S')\phi_S(S)\phi_S(S'). \tag{7}$$

The generalization of Eq. (3) for computing expectations of an operator $\hat{O}(R)$ with a SWF is

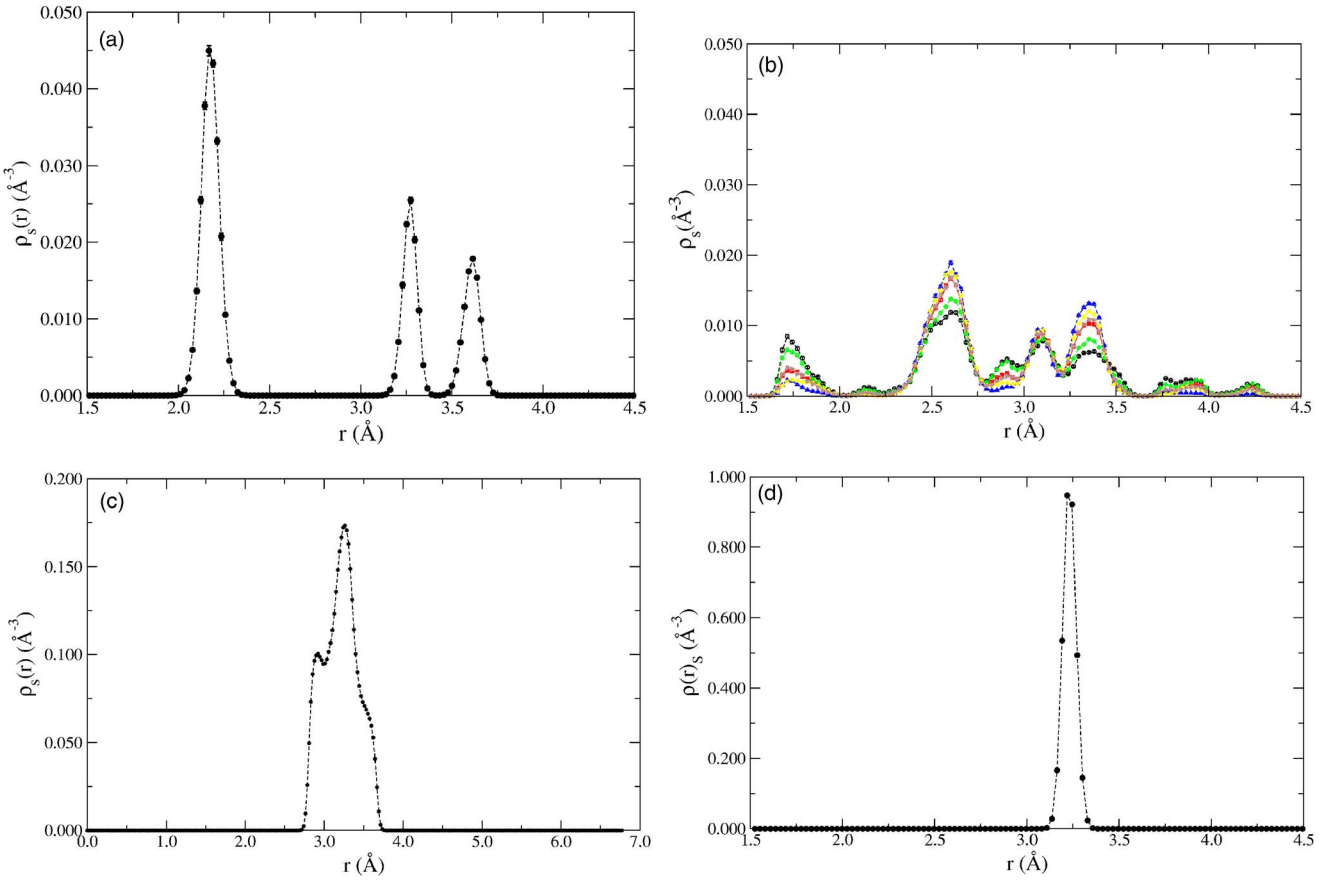

FIG. 3. (Color online) Nearest neighbors one-body densities $\rho_s(r)$ for shadows at $\rho=0.043\,00$ Å^{-3}. (a) density around a empty site for fcc crystal, (b) density around a empty site for hcp crystal, (c) density around a filled site for fcc crystal, (d) density around a filled site for hcp crystal. Results for fcc crystal are averaged over several MC runs.

$$\langle O\rangle = \frac{\int \Xi(R,S,S')\hat{O}(R)dRdSdS'}{\int \Xi(R,S,S')dRdSdS'} \sim \frac{1}{M}\sum_{l=1}^{M} O(R_l). \quad (8)$$

The most important features of SWF is that (i) it includes effects of correlations at any order beyond two-body by means of the auxiliary degrees of freedom, and (ii) crystalline order is stabilized without the need of one-body terms in the wave function, i.e., with a wave function which is explicitly translationally invariant. The last property makes SWF the ideal tool for studying properties of defective quantum crystals. In fact, the local structure self-consistently adapt to the variations in density. When using SWF, it is also possible to define operators depending on the auxiliary degrees of freedom S. Although such operators do not carry any real significant meaning, they are useful for analyzing the structure of the quantum crystal. In fact, as widely discussed in other works,[8,9] the shadows act as heavier particles indicating an "average" position for the real quantum particles. Therefore, operators depending on S can be used to determine the structure of the crystal effectively averaging most of the quantum fluctuations.

B. Simulations

We performed several sets of simulations a different densities (0.0215, 0.026, 0.043 Å^{-3}) and for two different lattices, hexagonal close packed (hcp) and face centered cubic (fcc). Simulation cells were set to accommodate $3\times3\times3$ elementary cubic cells for fcc, with a total of $N_l=108$ lattice sites, and $5\times3\times3$ elementary cells for a total of $N_l=180$ lattice sites for hcp. The vacancy is obtained by filling the cells with N_l-1 particles. The vacant site was chosen at random at the beginning of the simulation.

Each simulation consisted of sampling M configuration of the set (R,S,S'). In order to minimize the autocorrelation in the sampled configurations due to the harmonic correlations between particles and shadows, a new configuration is generated by displacing a trimer composed by a molecule and the corresponding shadows. The sampling algorithm was described in detail in Ref. 4.

The results were obtained computing average over 10^4 configurations dumped during the VMC simulation. The spacing among subsequent configurations is such that autocorrelation effects are strongly reduced.

We stress the fact that the simulations refer to a crystal at $T=0$, so no thermal effects are induced. The phenomenology is completely due to the strong quantum nature of the system.

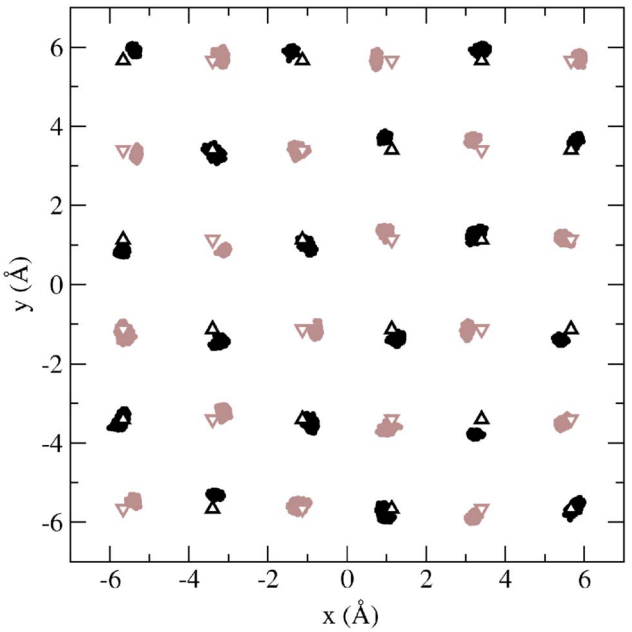

FIG. 4. (Color online) One body density of shadows in two 100 layers in a fcc crystal at density $\rho=0.043$ Å^{-3}. Triangles are the lattice sites. Black and gray spots refer to two different layers.

C. Position of the vacancy

As already mentioned, one of the most interesting properties of SWF is the fact that the crystalline order is stable even if the function is explicitly invariant under translations. A consequence of this property is that molecules can diffuse away from their original position in the lattice and exchange positions with other molecules. While this process is rather rare in the perfect crystal, the presence of a vacancy increases its frequency, because molecules can hop into the vacant site. We can interpret this hopping as delocalization of the vacancy in the crystal. Given the quantum nature of the system this phenomenon is expected to occur also at $T=0$. We have, therefore, to face the problem of localizing the vacancy in the crystal. If we divide the N-sites simulation cell in Voronoi sub-cells, typically only N-1 will have unitary occupancy, and one will be empty. The geometrical center of the empty cell is defined as current the position of the vacancy. However, the large vibrations of the molecules, particularly at low densities, can lead to empty sub-cells which are not representing a vacancy but rather a sort of interstitial vacancy pair (IVP). In this case, one of the nearest Voronoi sub-cells must be double occupied. We can, therefore, easily distinguish IVP from the real vacant site whenever they occur. Particular care must be taken in referring each configuration to the same origin. It can be seen that in this case the number of IVP can be made very small. The typical fraction we observed is between 2 and 6%.

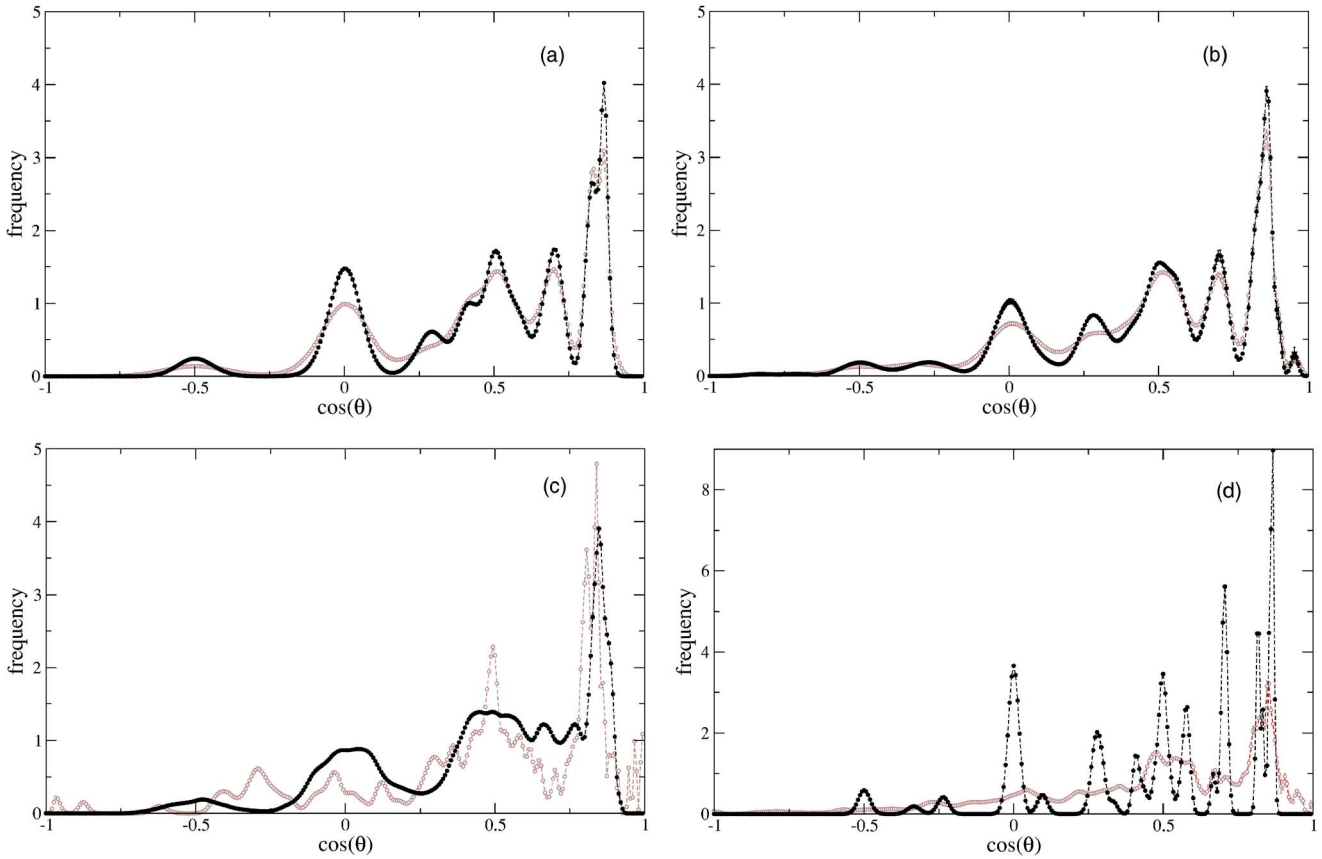

FIG. 5. (Color online) Average distribution of angles between nearest neighbors of empty (gray symbols) and filled (black symbols) sites: (a) fcc crystal at $\rho=0.026\,00$ Å^{-3}. (b) hcp crystal at $\rho=0.026\,00$ Å^{-3}. (c) fcc crystal at $\rho=0.043\,00$ Å^{-3}. (d) hcp crystal at $\rho=0.043\,00$ Å^{-3}.

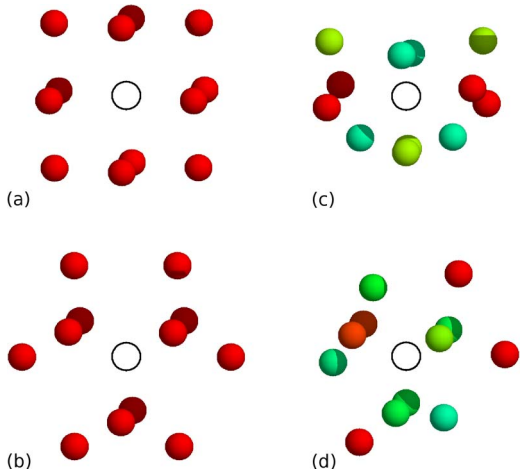

FIG. 6. (Color online) Mean positions of the first shell of *shadows* particles around a vacancy. Darker colors correspond to bigger distance from the central vacant site (empty circle). (a) fcc crystal at $\rho=0.026\,00$ Å^{-3}. (b) hcp crystal at $\rho=0.026\,00$ Å^{-3}. (c) fcc crystal at $\rho=0.043\,00$ Å^{-3}. (d) hcp crystal at $\rho=0.043\,00$ Å^{-3}.

III. RESULTS

A. Structural analysis

The density distribution of the nearest neighbors and next-nearest neighbors around occupied sites and vacancies for a hcp lattice at $\rho=0.021\,50$ Å^{-3} and $\rho=0.026\,00$ Å^{-3} are plotted in Fig. 1. All the results are averaged over ten independent MC runs. In the figures, the origin of the x axis represents the center of either a filled or a vacant Voronoi sub-cell. All the distributions calculated around the filled sites are very accurately fitted by a single Gaussian and peak at the expected distance of the first and second neighbors. Moreover, their integrals yield the correct number of neighbors. The plotted curves are all normalized to one.

At low density $\rho=0.021\,50$ Å^{-3}, the density of nearest-neighbors clearly relaxes into the empty site. This is expected because of the gain in kinetic energy obtained by broadening the wave function of the molecule. On the contrary, second neighbors are slightly shifted outwards. This might be a consequence of the broadening of the density of nearest neighbors which tend to subtract space to the second neighbors. The outwards shift becomes, therefore, energetically favored. The sharp cutoff located at half the nearest distance from the center of the vacancy is an artifact of the method used for localizing the vacancy, which constrains us to consider a site to be a vacancy only if the Voronoi cell is completely empty. Therefore, if one of the neighboring molecules of the vacancy relaxes in the vacant sub-cell, this is considered as a hop of the vacancy in another cell.

At the saturation density ($\rho=0.026\,00$ Å^{-3}) the one-body density of nearest-neighbors around the empty site becomes essentially Gaussian, and no strong asymmetry is observed.

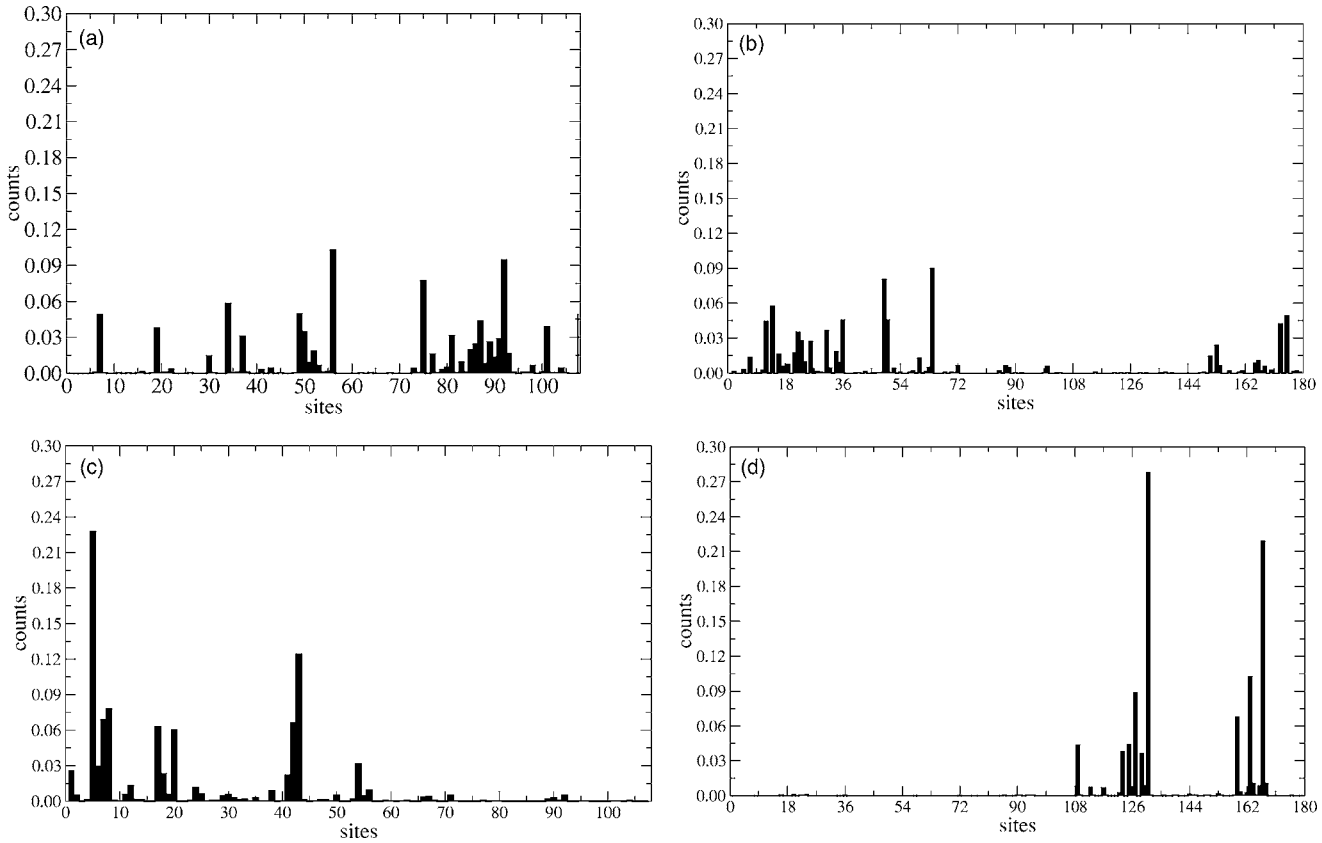

FIG. 7. The normalized frequency of occurrence of the vacancy for each lattice site. (a) $\rho=0.021\,50$ Å^{-3} (fcc crystal); (b) $\rho=0.021\,50$ Å^{-3} (hcp crystal); (c) $\rho=0.043\,00$ Å^{-3} (fcc crystal); (d) $\rho=0.043\,00$ Å^{-3} (hcp crystal). Analyzed configurations at $\rho=0.021\,50$ Å^{-3} are consecutive; configurations at $\rho=0.043\,00$ Å^{-3} are saved every 2000 MC steps.

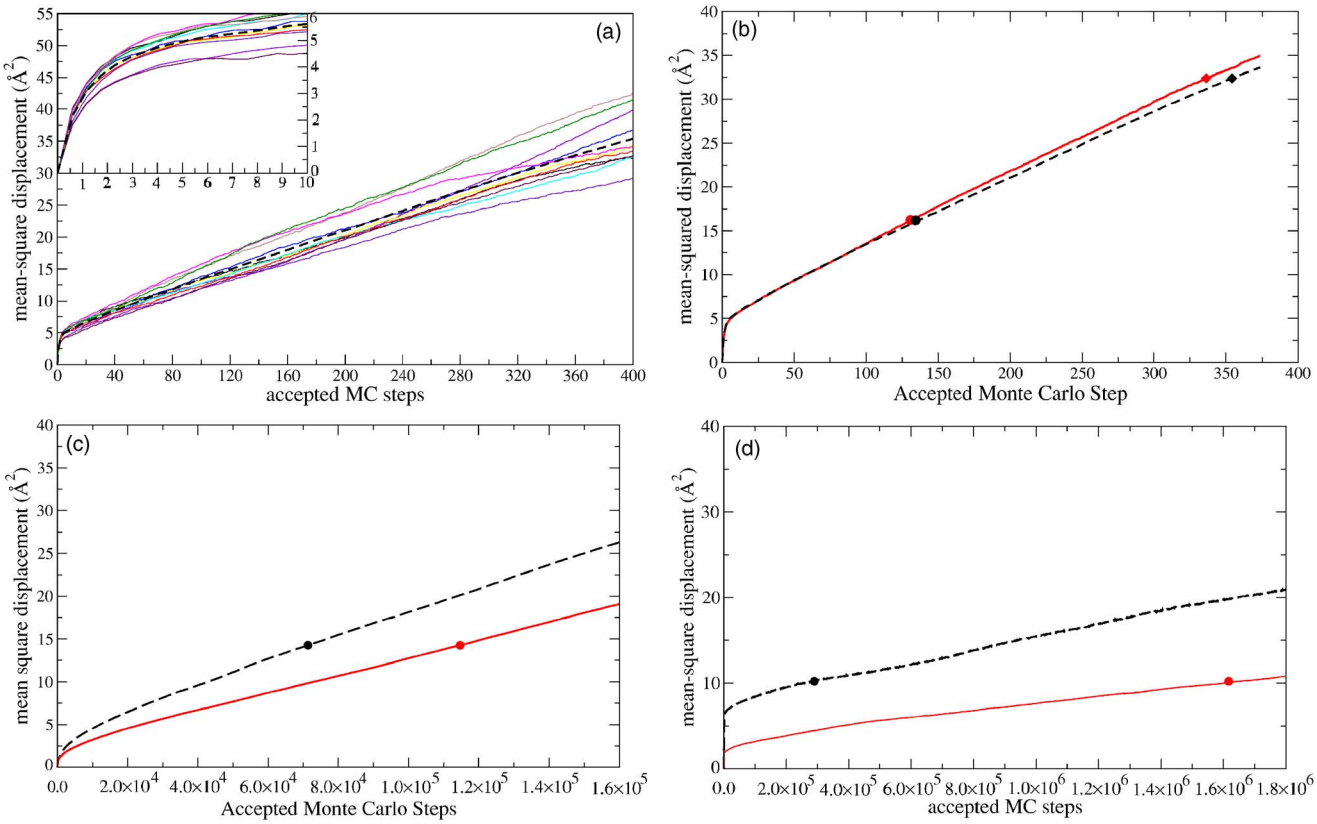

FIG. 8. (Color online) The mean-square displacement of a vacancy as a function of the number of MC accepted moves in the system. Graph (a) shows results of individual runs for a fcc crystal at $\rho=0.021\,50$ Å^{-3}. Different runs generated data with a fairly spread of values for the distance traveled. The average over these run is shown as a black dashed curve. In the other graphs are plotted the averaged mean-square displacement in the hcp (solid line) and in the fcc (dashed line) crystal at densities $\rho=0.021\,50$ Å^{-3} (b), $\rho=0.026\,00$ Å^{-3} (c), and $\rho=0.043\,00$ Å^{-3} (d). Filled circles and diamonds indicate the squared distance of the nearest and the next-nearest neighbors, respectively.

Relaxation effects are still observed in the shift of the peak and in the broadening of the Gaussian with respect to the density found around filled sites. A slight shift outwards of the next-near neighbors is also visible. In both cases, results for the fcc crystal were found to be nearly the same as for hcp.

In Fig. 2 we display the one-body densities for a higher density crystal ($\rho=0.043\,00$ Å^{-3}) for several different MC runs. While it is classically expected that relaxation effects are less significant at higher densities, all the curves show that the nearest neighbors distribution tends again to shift drastically into the vacant site. The shape of the computed densities varies very strongly from run to run, but in nearly all the cases it is no longer Gaussian, both in the hcp and in the fcc crystal.

Some simulations in the fcc lattice show also a density with a marked new peak closer to the minimum neighbors distance, giving an indication of a possible appearance in the simulated system of a different ordered structure around the vacant site. A clearer picture of the deformation of the crystal around an empty site can be obtained by looking at the behavior of the shadow degrees of freedom. As already mentioned, shadows behave as markers of the average position of the real particles, which are highly delocalized due to quantum fluctuations. The analysis of the density of shadows around the vacant site allows for having a cleaner picture of the ordered structure underlying the motion of the molecules. This is particularly useful at high density, in order to investigate if distortions of the lattice structure occur.

In Fig. 3 we show the density of shadows which are nearest neighbors of filled sites (in the crystal with no vacancies) and of the vacancy for simulations in both fcc and hcp crystals.

An interesting feature that can be observed is the formation of multiple peaks in the density of nearest neighbors of the filled site in the fcc crystal, to be compared with the almost perfect Gaussian density observed in the hcp. This behavior is always reproduced. In order to understand its origin, we investigated the one-body density of shadows by plotting their positions dumped from a simulation segment of 1000 steps and looking at (100) layers in the crystal. An example of our results is given in Fig. 4, where it can be clearly seen that the (100) layers appear to be strained. A reason for this behavior might be the tendency of the system to evolve towards a packing of (111) layers (which do not fit in our cubic simulation box), indicating that the fcc order is unstable at this density. The distortion of the planes is compatible with the appearance of multiple peaks in the nearest neighbors density. As expected, no distortions have been found in the hcp crystal, which is known to be stable in this range of densities.

In general, it can be noticed that the density of shadows around filled sites is much more peaked than the correspond-

ing density of particles. This well illustrates the more "classical" character of the auxiliary degrees of freedom. The density around the vacancy clearly shows a series of peaks which have little to do with the expected single-Gaussian distribution. In particular, in both cases it is possible to observe a splitting of the average position of the shadows among multiple peaks at different distance from the lattice site. In the simulations of the hcp crystal, different MC runs converging to the same energy value yield different density profiles [Fig. 3(b)] for molecules surrounding the vacant sites. However, all profiles are characterized by the same series of peaks. The distribution of the density among the peaks varying from run to run can probably be interpreted as an indication that the nearest neighbors shell of a vacant site can be found in more than one energetically equivalent structure. A consistent behavior is shown by the mean distributions of angles between nearest neighbors of empty and filled sites (Fig. 5) defined as

$$\Theta(\cos(\theta)) = \left\langle \sum_{\langle nn \rangle} \delta\left(\cos(\theta) - \frac{\mathbf{r}_i \cdot \mathbf{r}_j}{r_i r_j}\right) \right\rangle. \tag{9}$$

At equilibrium density no substantial differences are found between empty and filled WS cells. At higher densities these differences become substantial. In the simulations of the hcp crystal, the positions and the heights of the peaks of the angular distribution of nearest neighbors of filled sites are consistent with the structure of the lattice. On the contrary, the peaks are only minimally reproduced by the angular distribution computed around empty sites, giving a further indication that the structure of the WS cell containing a vacancy is no longer preserved. In the case of the fcc crystal, the peaks in the angular distribution computed around filled sites are no longer well-defined, probably due the observed straining of the (100) planes of the lattice, while shadows surrounding empty cells seem to arrange in a well-defined structure different from the fcc one. In order to visualize the such differences between angular distributions around empty and filled Voronoi cells, we computed the mean position of neighbors of a fixed vacant site throughout the simulation and compared them with averaged positions of neighbors of filled sites. Pictures in Fig. 6 show mean positions of nearest neighbors of a vacant site calculated using *shadows* coordinates.

At $\rho=0.026\,00$ Å^{-3} the arrangement of the molecules is perfectly consistent with the lattice structure analyzed. The same result was obtained using the coordinates of the molecules instead of those of the *shadows*. At $\rho=0.043\,00$ Å^{-3} the deformation of the geometry of molecules surrounding the empty cells becomes evident, in particular when considering *shadows* coordinates. It looks like the nearest neighbors tend to be squeezed into the vacancy to gain more room and lowering, therefore, their kinetic energy. In the case of fcc lattice, the new structure formed around the empty site by the shadows is well defined, forming two penetrating tetrahedral shells, with the remaining four molecules occupying the remaining interstitials. It should be noted that the fact that the fcc lattice is unstable might interfere with the local distortions induced by the vacancy, and may favor the formation of the well-defined structure surrounding it. From this point of view the physically meaning result is given by the presence of the same distortions in the simulations of the hcp crystal, although, in this case, the structure around the empty site appears to be not as well defined as in the case of the fcc lattice.

TABLE I. MC diffusion coefficients in Å^{-2} as function of density for fcc and hcp lattice.

ρ	fcc	hcp
0.021 50	7.7097×10^{-2}	8.0341×10^{-2}
0.026 00	1.3913×10^{-4}	1.0154×10^{-4}
0.043 00	9.0731×10^{-6}	6.8424×10^{-6}

B. Delocalization of vacancies

Since we are able to track the position of the vacancy throughout a MC run, we can count how many times the vacancy is localized on each lattice site during the run (Fig. 7). We also computed the mean-square distance "traveled" by the vacancy in our simulations as function of the number of MC configurations sampled (Fig. 8). Clearly such motion has no direct physical meaning, but rather as an indication of the fact that the vacancy can be displaced from the initial position as an effect of the quantum fluctuations present in the system. Therefore, it is misleading to think of subsequent positions sampled for the vacancy as an effective trajectory in time. Nevertheless, the motion we observe in our MC simulations can be suggestive of some properties of the vacancies in fcc and hcp lattices. The amount of displacement varied somewhat from run to run. We could obtain accurate data by averaging across several independent runs for each studied density value. The long linear portion of all curves shows that after a certain number of accepted MC steps, the displacement of the vacancy follows a diffusive regime. The values of the fitted diffusion coefficients are shown in Table I. These values decrease drastically by incrementing the density, due the stronger localization of the molecules close the lattice sites. Nevertheless, in all the simulations performed we could observe that the vacancy moved from initial position beyond the first shell of neighbors, and such delocalization of the vacancy still remained at high density both for hcp and fcc lattices, as shown also by Fig. 7. At low density ($\rho=0.021\,50$ Å^{-3}) results of the MC diffusion coefficient for fcc and hcp are almost the same. At higher densities instead, the diffusion coefficient in the simulations for the hcp lattice is more than 30% smaller than that obtained for fcc lattice, and a strong difference in the initial portion of the curves is seen. This means that the average amount of sampled configurations needed in order to find the vacancy in a nearest neighbor site is two to four times smaller for the strained fcc lattice. The latter structure seems to allow a bigger vacancies mobility at high densities than the hcp one. This observation is in agreement with the analysis of the density profiles discussed in the previous section. As shown in Fig. 2, the density near the empty cell boundary is much higher in the fcc crystal than in the hcp. Therefore, a surrounding molecule is

more likely to cross over the boundary filling the empty site and moving the vacancy out.

IV. CONCLUSIONS

We have performed a systematic analysis of the effects of a presence of a vacancy in a p-H_2 crystal by means of variational Monte Carlo simulations based on shadow wave functions. Vacancies at low densities appear to be quite delocalized. The corresponding distortion of the lattice structure is limited to a relaxation of the nearest neighbors into the vacant site, as already predicted by simulations in ^{4}He. The results at high densities are instead partly unexpected. While the vacancy becomes more localized due to the increased rigidity of the crystal, it gives rise to a strong deformation of the structure of the nearest neighbors, which loose completely the icosahedral symmetry and tend shift into the vacancy.

ACKNOWLEDGMENTS

We thank G. Galli, M. H. Kalos, and G. V. Chester for useful discussions. This work was performed in part on the computational facilities at CINECA under an INFM-ICP grant, and in part on the cluster at ECT* as an approved supercomputing research project.

[1] D. E. Galli, M. Buzzacchi, and L. Reatto, J. Chem. Phys. **115**, 10239 (2001).
[2] D. Galli and L. Reatto, Phys. Rev. Lett. **96**, 165301 (2006).
[3] M. Boninsegni, A. B. Kuklov, L. Pollet, N. V. Prokof'ev, B. V. Svistunov, and M. Troyer, Phys. Rev. Lett. **97**, 080401 (2006).
[4] F. Pederiva, G. V. Chester, S. Fantoni, and L. Reatto, Phys. Rev. B **56**, 5909 (1997).
[5] B. Chaudhuri, F. Pederiva, and G. V. Chester, Phys. Rev. B **60**, 3271 (1999).
[6] D. Zhou, C. M. Edwards, and N. S. Sullivan, Phys. Rev. Lett. **62**, 1528 (1989).
[7] M. Rall, D. Zhou, E. G. Kisvarsanyi, and N. S. Sullivan, Phys. Rev. B **45**, 2800 (1992).
[8] S. Vitiello, K. Runge, and M. H. Kalos, Phys. Rev. Lett. **60**, 1970 (1988).
[9] L. Reatto and G. L. Masserini, Phys. Rev. B **38**, 4516 (1988).
[10] D. E. Galli and L. Reatto, J. Low Temp. Phys. **134**, 121 (2004).
[11] R. A. Guyer, J. Low Temp. Phys. **8**, 427 (1972).
[12] F. Operetto and F. Pederiva, Phys. Rev. B **69**, 024203 (2004).
[13] I. F. Silvera and V. V. Goldman, J. Chem. Phys. **69**, 4209 (1978).
[14] F. Operetto and F. Pederiva, Phys. Rev. B **73**, 184124 (2006).